A comparative study of the crystallographic, magnetic and electrical properties of the $Nd_{1-x}La_xNiO_{3-delta}$ system

1994 J. Phys.: Condens. Matter 6 10759

(http://iopscience.iop.org/0953-8984/6/49/017)

J. Phys.: Condens. Matter 6 (1994) 10759–10772. Printed in the UK

A comparative study of the crystallographic, magnetic and electrical properties of the $Nd_{1-x}La_xNiO_{3-\delta}$ system

J Blasco and J García

Instituto de Ciencia de Materiales de Aragón, CSIC-Universidad de Zaragoza, Facultad de Ciencias, Plaza San Francisco s/n, 50009 Zaragoza, Spain

Received 26 July 1994

Abstract. The synthesis and physical characterization of $Nd_{1-x}La_xNiO_{3-\delta}$ (from $x = 0$ to 1) samples are reported. $Nd_{1-x}La_xNiO_{3-\delta}$ samples are orthorhombic for $x \leqslant 0.4$ and rhombohedral for $x > 0.4$. Resistivity and magnetic susceptibility measurements from 4.2 K to 300 K are also reported. The increase of La content up to $x = 0.4$ induces the decrease of metal–insulator (MI) phase transition temperature and compounds with $x \geqslant 0.5$ are metallic. The distortion degree of the ideal perovskite structure, directly related to the Ni–O–Ni angle, is correlated with the MI phase transition temperature. The metallic phase is characterized by a linear dependence of $\rho(T)$ with a residual resistivity that decreases with x, being near zero for $LaNiO_3$. The conductivity in the semiconducting phases at low temperatures follows a variable-range hopping mechanism. The magnetic susceptibility shows a Curie–Weiss contribution from the Nd sublattice and a Pauli susceptibility of similar magnitude for all samples. The analysis of the experimental data shows large electronic correlations in these compounds.

1. Introduction

The study of $RENiO_3$ oxides with perovskite-like structure has received renewed interest in the last few years [1–5]. This must be related to the discovery of high-temperature superconductivity in the perovskite-like copper oxides and to their outstanding electronic properties. While $LaNiO_3$ is metallic down to 1.7 K, $RENiO_3$ compounds, with RE = Pr, Nd, Sm and Eu, present a metal–insulator (MI) phase transition at different temperatures [2, 6]. The electronic properties of transition metal oxides have been described in the well known Zaanen–Sawatsky–Allen phase diagram [7]. Insulating $RENiO_3$ compounds have been located in the charge transfer region of the former phase diagram [6, 8]. Recently, spectroscopy results and density of states calculations have suggested that MI phase transitions in this system arise from changes in the conduction bandwidth [9]. Therefore, the metallic or insulator behaviour in these compounds has been related to the Ni–O–Ni bond angle, which controls the conduction bandwidth of O 2p and Ni 3d parentage. This angle is close to 180° in $LaNiO_3$ sample and decreases as the rare earth (RE) size diminishes in the $RENiO_3$ series. Moreover, neutron diffraction experiments have shown that long-range magnetic ordering is simultaneous with the MI phase transition for $NdNiO_3$ and $PrNiO_3$ samples, giving a spin density wave [10].

Nevertheless, the magnetic and electronic states of these systems are matters of controversy and several questions remain unanswered. Surprisingly, no appreciable discontinuity in the magnetic susceptibility curve is observed at the transition temperature [11, 12] and the entropy associated with the phase transition cannot be ascribed to an Ni spin $\frac{1}{2}$ sublattice ordering [12]. Moreover, x-ray absorption results [8, 13], at temperatures

0953-8984/94/4910759+14$19.50

below the MI transition, disagree with a +3 oxidation state for the Ni atom as expected from the nominal stoichiometry.

The study of the $Nd_{1-x}La_xNiO_3$ series can give important keys in the understanding of the basic electronic properties in these oxides. On the one hand, $LaNiO_3$ is a metallic system with an enhanced temperature independent magnetic susceptibility that has been explained in the framework of a spin polaron model [14, 15]. On the other hand, $NdNiO_3$ shows an MI transition at 205 K and its magnetic susceptibility follows a Curie–Weiss-like behaviour. Two magnetic contributions have been observed: the Curie–Weiss contribution from the Nd sublattice and a temperature independent contribution of similar magnitude to that of $LaNiO_3$ [12, 16]. Both oxides show a linear behaviour of the resistivity in the metallic state at high temperatures, suggesting a similar polaron mechanism of conduction for both compounds [12].

The substitution of Nd by La in the $NdNiO_3$ system would induce several effects. First, a change in the unit cell from orthorhombic $NdNiO_3$ to rhombohedral $LaNiO_3$ as a function of substitution degree is expected. Second, the behaviour of the MI transition temperature as a function of the composition will provide an MI phase diagram for this material related to the rare earth site or perovskite distortion. Third, the substitution of rare earth magnetic Nd^{3+} by the diamagnetic La^{3+} ion could make more significant the Ni magnetic state due to the decrease of the Nd paramagnetic contribution.

In this work we present the physical characterization of the $Nd_{1-x}La_xNiO_{3-\delta}$ (from $x = 0$ to 1) samples synthesized using a sol–gel method [11, 17]. The change from the orthorhombic phase to the rhombohedral phase, the electrical behaviour from 4.2 K to 300 K and the temperature dependence of the magnetic susceptibility has been also determined for all the samples.

2. Experimental details

Samples with nominal composition $Nd_{1-x}La_xNiO_{3-\delta}$ ($x = 0$, 0.1, 0.2, 0.3, 0.4, 0.5, 0.6, 0.75, 0.9, 1) were prepared using a sol–gel method described elsewhere [17, 18].

The pellets were black and they showed a high electrical conductivity at room temperature that decreased as the Nd content in the sample increased. All the samples were characterized as pure phases by means of the x-ray powder diffraction technique. The x-ray diffraction patterns were obtained at room temperature on a D-max Rigaku system. They were collected in the range of $19° < 2\theta < 80°$.

Determination of the O content in the samples was carried out by thermogravimetric analysis (TGA) in a reducing atmosphere, using a Perkin–Elmer system. The atomic ratios of Ni, Nd and La in the samples were determined by fluorescence analysis using a Jeol JSM-6400 electron microscope and a Link Analytical EDS x-ray spectrometer. The analysis was performed over polished bulk samples with an accelerating voltage of 20 keV. The atomic ratio La:Nd:Ni always coincides with the nominal value calculated for all samples. We have noted that this synthetic method guarantees the homogeneous distribution of Nd and La. Density measurements of the pellets were made using the Archimedes method. All samples had densities around 60–70% of the theoretical value.

Magnetic and resistance measurements as a function of temperature were performed in a temperature controlled multipurpose cryostat from 4.2 K to 300 K. The AC magnetic susceptibility was found through the determination of magnetic flux variation in a pick-up coil system [19]. Electrical resistance was measured over bars ($1.5 \times 1.5 \times 5.5$ mm^3) cut from the pellets using a four-probe AC (20 Hz) method.

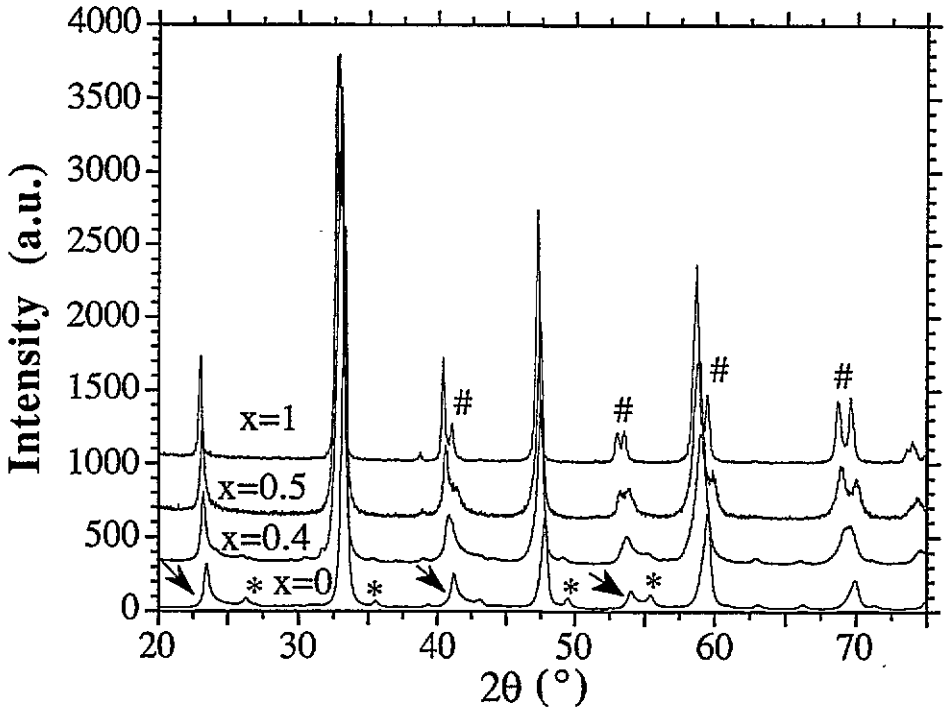

Figure 1. XRD patterns of several $Nd_{1-x}La_xNiO_{3-\delta}$ samples (x is given for each pattern). * and # indicate some characteristic diffraction peaks of orthorhombic and tetragonal unit cells respectively. The arrows show diffraction peaks with anomalous broadening.

Table 1. Lattice parameters, space groups, O content ($3-\delta$) and grain size for $Nd_{1-x}La_xNiO_{3-\delta}$ samples.

Sample	a (Å)	b (Å)	c (Å)	Space group	$3-\delta(\pm 0.03)$	Size (Å)
$NdNiO_{3-\delta}$	5.415	5.376	7.609	*Pbnm*	2.91	350
$Nd_{0.9}La_{0.1}NiO_{3-\delta}$	5.392	5.345	7.626	*Pbnm*	2.89	370
$Nd_{0.8}La_{0.2}NiO_{3-\delta}$	5.399	5.372	7.635	*Pbnm*	2.90	420
$Nd_{0.7}La_{0.3}NiO_{3-\delta}$	5.403	5.377	7.644	*Pbnm*	2.88	400
$Nd_{0.6}La_{0.4}NiO_{3-\delta}$	5.419	5.373	7.665	*Pbnm*	2.92	380
$Nd_{0.5}La_{0.5}NiO_{3-\delta}$	5.429	—	13.081	$R\bar{3}c$	2.92	480
$Nd_{0.4}La_{0.6}NiO_{3-\delta}$	5.436	—	13.067	$R\bar{3}c$	2.99	600
$Nd_{0.25}La_{0.75}NiO_{3-\delta}$	5.432	—	13.033	$R\bar{3}c$	2.98	640
$Nd_{0.1}La_{0.9}NiO_{3-\delta}$	5.455	—	13.142	$R\bar{3}c$	2.98	620
$LaNiO_{3-\delta}$	5.454	—	13.136	$R\bar{3}c$	2.99	700

3. Results

3.1. Structural results

X-ray powder diffraction (XRD) patterns of $Nd_{1-x}La_xNiO_3$ ($x = 0$, 0.5, 0.6 and 1) are shown in figure 1. The patterns show single-phase systems and no impurity phases such as NiO, RE_2O_3 or RE_2NiO_4 (RE = La, Nd) were detected. They can be reasonably indexed either as the $NdNiO_3$ (orthorhombic *Pbnm*) structure or as the $LaNiO_3$ (rhombohedral $R\bar{3}c$) one,

depending on the Nd:La ratio. The lattice parameters and space groups are summarized in table 1. We have noted that the unit cell changes from orthorhombic to rhombohedral in the series between $x = 0.4$ and $x = 0.5$. This change is evidenced by the disappearance of some diffraction peaks, which are characteristic of the orthorhombic distortion (around 26°, 35° and 49° for example), from samples with $x = 0.5$. This sample shows a diffraction pattern similar to the rhombohedral $LaNiO_3$, as can be observed in figure 1.

SEM observations in different regions and simultaneous EDS analysis show a good homogeneity in the samples and the Nd/La ratio coincides with the nominal composition. The change in the unit cell can be related to the large La^{3+} ionic size and is in agreement with previous works and the Goldsmith tolerance factor [1–5].

The diffraction patterns show broad peaks due to the small grain size of the sample, which can be related to the low sintering temperatures used in the synthesis. The grain size of the samples was determined from the full width at half maximum (FWHM) of the XRD peaks by using the Scherrer equation. The results are summarized in table 1 and it is inferred that an increase of La content gives samples with larger grain size. Another characteristic of this system is the presence of some diffraction peaks in $NdNiO_3$ showing an anomalous broadening with a gradual fall-off in intensity on the high-angle side (see figure 1). The shapes of these peaks are similar to that reported for a system with laminar disorder in its structure [20]. The replacement of Nd by La diminishes the anomalous broadening, which disappears for $x > 0.5$ samples. This feature seems to be related to the O content in the samples. TGA measurements have been used to analyse the O content and the results have been summarized in table 1. The $NdNiO_{3-\delta}$ sample is O deficient ($\delta \approx 0.09$) while $LaNiO_3$ is stoichiometric. The O deficiency and the anomalous broadening decrease as the La content is increased in the sample. These samples are now being studied by means of TEM to perform a detailed study of the defects in the structure originated by the O deficiency and it will be the subject of a separate work. We only want to point out here that electron diffraction confirms the perovskite structure for all samples and stacking faults have been detected in the crystallographic planes, which show asymmetric peaks in the x-ray patterns.

Table 2. Magnetic constants obtained by fitting the curves of figure 3 to the equation $\chi = \chi_0 + C/(T - \theta)$ for $Nd_{1-x}La_xNiO_3$ samples between 100 K and 300 K.

	Experimenta data				Theoretical μ_{eff} (μ_B)	
Sample	C (emu K g^{-1}) ($\times 10^{-3}$)	θ (K)	χ_0 (emu g^{-1}) ($\times 10^{-6}$)	μ_{eff} (μ_B)	Nd^{3+}	$Nd^{3+} + Ni^{3+}$
$NdNiO_{3-\delta}$	6.38	−53.3	3.87	3.57	3.61	4.02
$Nd_{0.7}La_{0.3}NiO_{3-\delta}$	4.88	−55.04	2.68	3.09	3.02	3.50
$Nd_{0.5}La_{0.5}NiO_{3-\delta}$	2.79	−38.1	3.47	2.35	2.55	3.10
$Nd_{0.25}La_{0.75}NiO_{3-\delta}$	1.45	−46.5	2.61	1.69	1.80	2.52
$Nd_{0.1}La_{0.9}NiO_{3-\delta}$	0.997	−69.3	3.09	1.40	1.15	2.09
$LaNiO_3$	—	—	3.40	—	—	—

3.2. AC magnetic susceptibility

$1/\chi_{AC}$ curves as a function of temperature are shown in figure 2. While $NdNiO_{3-\delta}$ presents a Curie–Weiss-like behaviour, $LaNiO_3$ shows the characteristic temperature independent behaviour above 40 K and a rise in the paramagnetic signal at lower temperatures, as reported elsewhere [14, 16]. The magnetic properties of this oxide have been explained as

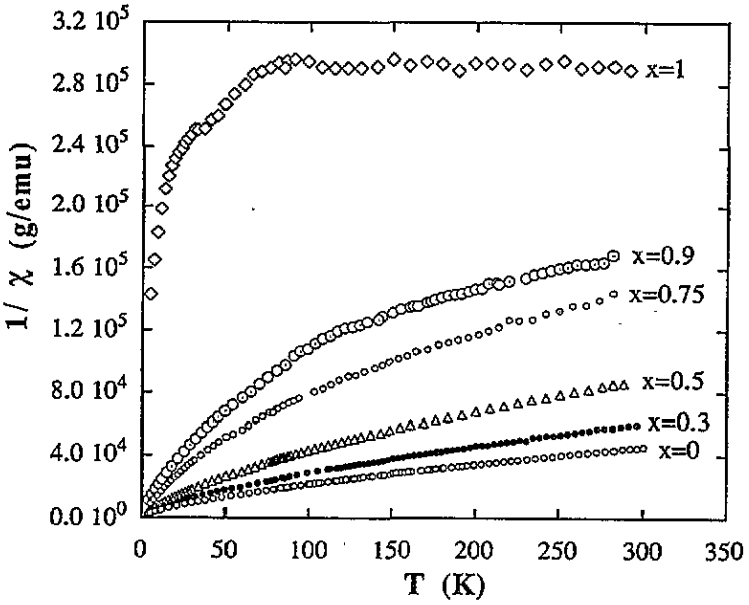

Figure 2. The inverse of the magnetic susceptibility versus temperature for the $Nd_{1-x}La_xNiO_{3-\delta}$ series.

due to the Pauli paramagnetism of itinerant electrons enhanced by ferromagnetic correlations [15]. The $Nd_{1-x}La_xNiO_{3-\delta}$ samples show two magnetic contributions: the Nd sublattice paramagnetism and the Pauli paramagnetism. The magnetic constants obtained from the fit of experimental data to the law $\chi = \chi_0 + C/(T-\theta)$ are summarized in table 2. Due to the crystal field splitting of the Nd^{3+} free ion ($J = \frac{9}{2}$), the temperature range of the fit was performed between 100 K and 300 K, well above the experimental temperatures found for thermal depopulation of the Nd^{3+} ground state in related oxides [11]. The calculated effective magnetic moment (μ_{eff}) agrees with the theoretical one calculated from the Nd sublattice without any contribution of the Ni sublattice in this temperature range despite electronic localization at 205 K (see table 2). The value of the χ_0 parameter is similar for all samples and coincides with the constant susceptibility of $LaNiO_3$, indicating similar values of Pauli paramagnetism for the whole system and, therefore, similar correlations of itinerant electrons.

3.3. Transport properties

Resistivity curves against temperature for the $Nd_{1-x}La_xNiO_{3-\delta}$ system in cooling and heating cycles are shown in figure 3. $NdNiO_{3-\delta}$ shows an MI transition with a large thermal hysteresis as described elsewhere [12]. The partial replacement of Nd by La ($x \leqslant 0.3$) lowers the MI transition temperature from 205 K to 120 K and decreases the hysteresis range. The hysteresis disappears for higher La substitution but a minimum in the resistivity curve (around 15 K) is found for $x = 0.4$. The sample with $x = 0.5$ exhibits metallic behaviour down to 6 K and its resistivity is constant below this temperature. Compounds with higher La content show metallic behaviour down to 4.2 K.

The samples that present the MI phase transition show a thermal hysteresis behaviour similar to that reported for $NdNiO_{3-\delta}$ [17] as can be observed, for example, for the

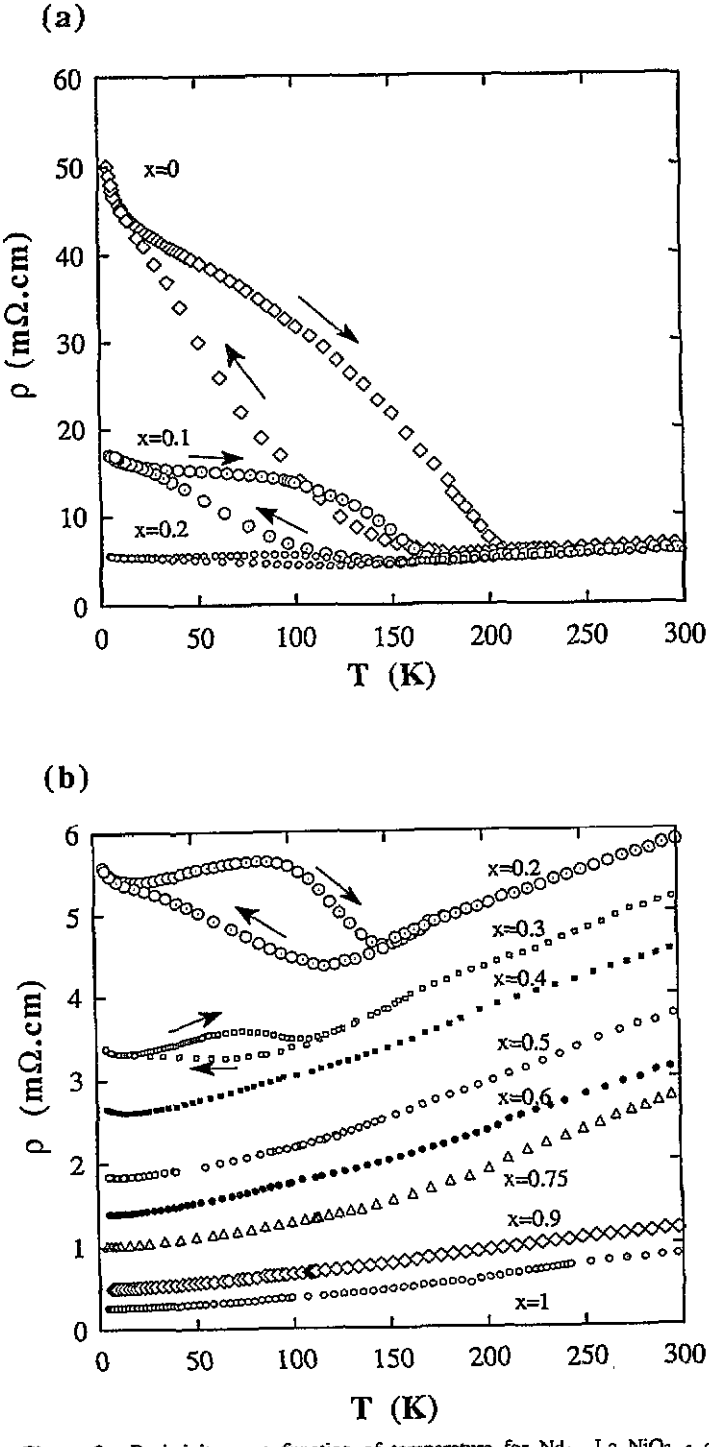

Figure 3. Resistivity as a function of temperature for $Nd_{1-x}La_xNiO_{3-\delta}$ compounds: (a) $0 \leqslant x \leqslant 0.2$ and (b) $0.2 \leqslant x \leqslant 1$.

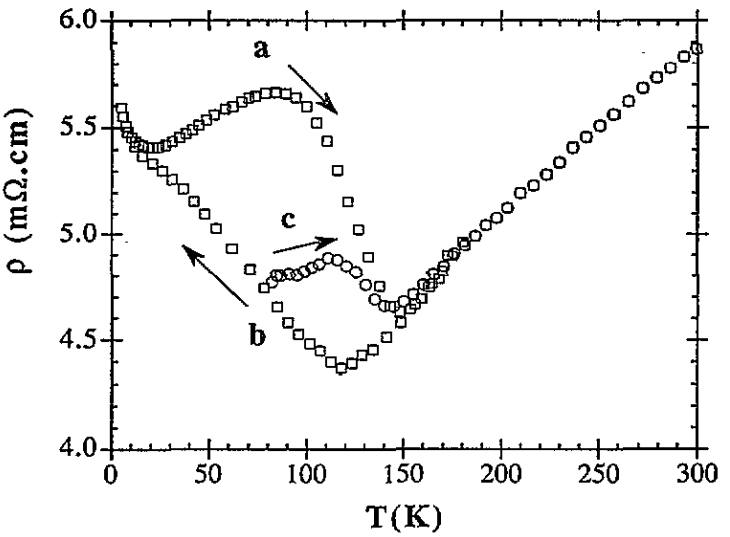

Figure 4. Resistivity $\rho(T)$ curves showing the hysteresis behaviour of the MI transition in the $Nd_{0.8}La_{0.2}NiO_{3-\delta}$ sample. The arrows indicate the thermal direction run along the measures. Circle points are obtained by heating after cooling the sample to 77 K.

$Nd_{0.8}La_{0.2}NiO_{3-\delta}$ sample in figure 4. When the sample is heated from 4.2 K, the resistivity follows curve **a** with a sharp MI transition at 145 K. If the heating is stopped at lower temperatures than the MI transition and the sample is cooled, the resistivity follows the same curve **a**. However, when the sample is cooled down from room temperature, the resistivity leaves curve **a** at 145 K and follows curve **b** down to 15 K, where the two curves join again. If the cooling is interrupted below 120 K (the temperature of minimum resistivity in the cooling run) and the temperature is raised again, the resistivity does not follow the same curve **b** and new cycles appear. The behaviour of the resistivity when the sample is cooled down to 77 K and heated again (curve **c**) can be seen in figure 4. These results show that the transition from the non-metal to metal state is sharp, but, the transformation in cooling runs extends over a large temperature range and two phases coexist.

Furthermore, a change of the slope sign of the $\rho(T)$ curve in the insulator phase is also observed for the $x = 0.2$ and $x = 0.3$ samples in the heating run with a minimum around 20 K (see figure 3(b)). This behaviour is similar to that described for the mobility of a small polaron [21] and similar to resistance curves reported for $PrNiO_3$ under high pressure [1, 22]

3.3.1. Metallic phase. A linear temperature dependence of the resistivity in the metallic phase at high temperatures (> 150 K) is observed in the whole series. For the metallic samples ($x > 0.4$) the resistivity curve shows a continuous curvature at low temperatures (see figure 3(b)). At temperatures higher than 150 K, the resistivity follows a linear law, $\rho = \rho_0 + AT$. This behaviour is also observed in the metallic phase for samples with the MI phase transition. For $LaNiO_3$ the linear resistivity extrapolates close to the origin ($\rho_0 \approx 0.02$ mΩ cm), whereas an increasing residual resistivity, ρ_0, is observed at higher Nd content. These results are in agreement with recent results reported on $LaNiO_3$ oxide [11, 23, 24] and this law has been also observed in high-temperature superconductors above T_c. A diffusion motion of spin polarons (or bipolarons) that follows the Einstein relation

has been suggested by Mott [25]:

$$\sigma = Nq^2D/kT \tag{1}$$

where the diffusion coefficient D is temperature independent.

Low values of residual resistivity (ρ_0) are expected for systems with diffusive motion of spin polarons [26], and, consequently, our experimental results are in agreement with the hypothesis of a ferromagnetically coupled gas of spin polarons for $LaNiO_3$ described elsewhere [14, 15]. On the other hand, Mott suggests that large values of ρ_0 indicate scattering by disorder resulting in a behaviour of the carriers as normal heavy particles [26]. This might explain the increase of ρ_0 in samples with high Nd content. The disorder can have several origins with increasing Nd content: (i) the increase of O vacancies in the lattice, (ii) the higher orthorhombic distortion of the unit cell and (iii) the higher contribution of the grain boundaries due to the lower grain size. The contributions (i) and (ii) would be, in our opinion, the most important ones because samples with different grain sizes show similar electrical behaviour [17].

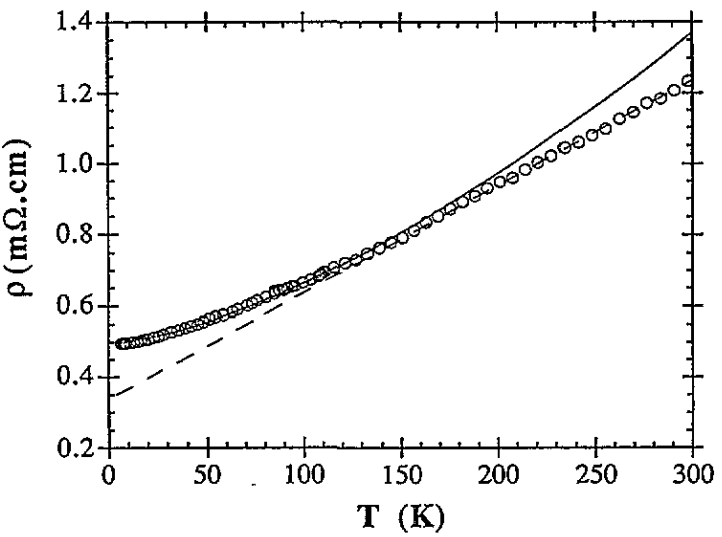

Figure 5. The resistivity of the $Nd_{0.1}La_{0.9}NiO_{3-\delta}$ sample and the fits to the $\rho = \rho_0 + AT$ law (– – –) and the $\rho = \rho_A + BT^{3/2}$ law (——).

The best fit for resistivity at low temperatures yields a power law: $\rho = \rho_A + BT^{3/2}$ in metallic samples (without an MI transition). This behaviour can be clearly seen in figure 5 where the resistivity of $Nd_{0.1}La_{0.9}NiO_3$ against temperature has been plotted together with the two fits obtained: linear dependence for high temperatures and $T^{3/2}$ dependence for low temperatures. Similar results have been obtained for samples with $x \geqslant 0.5$. The $T^{3/2}$ temperature dependence has been recently observed in $LaNiO_{3+\delta}$ ($\delta = 0.2$) [16] and it might indicate the prevalence of dielectric forces and scattering by phonons in this temperature range. The best fit parameters in both temperature ranges are summarized in table 3.

The series shows an increase of resistivity with the Nd content at 300 K (see table 3). Considering a metallic band of Ni e_g^* parentage and the contribution of one electron per Ni^{3+} ion, all the samples must have the same carrier number and the differences in the

Table 3. A comparison of several electronic parameters of $Nd_{1-x}La_xNiO_{3-\delta}$ oxides.

Sample (x)	$\rho_{300\ K}$ (mΩ cm)	$\rho_{300\ K}/\rho_{4.2\ K}$	ρ_0 (mΩ cm)	$1/\rho\ d\rho/dT$ (K^{-1})	ρ_A (mΩ cm)	B (mΩ cm $K^{-3/2}$)
0	6.7	0.13	4.1	1.5×10^{-3}	—	—
0.1	6.2	0.36	3.6	1.5×10^{-3}	—	—
0.2	5.9	1.05	3.5	1.4×10^{-3}	—	—
0.3	5.2	1.5	2.6	1.8×10^{-3}	—	—
0.4	4.5	1.5	2.3	1.6×10^{-3}	2.97	5.6×10^{-4}
0.5	3.7	2.05	1.3	2.5×10^{-3}	1.82	3.7×10^{-4}
0.6	3.0	2.14	0.8	2.8×10^{-3}	1.39	3.7×10^{-4}
0.75	2.8	2.6	0.4	3.0×10^{-3}	1.02	2.8×10^{-4}
0.9	1.2	2.45	0.3	2.8×10^{-3}	0.49	1.8×10^{-4}
1.0	0.9	3.0	0.02	3.5×10^{-3}	0.25	1.1×10^{-4}

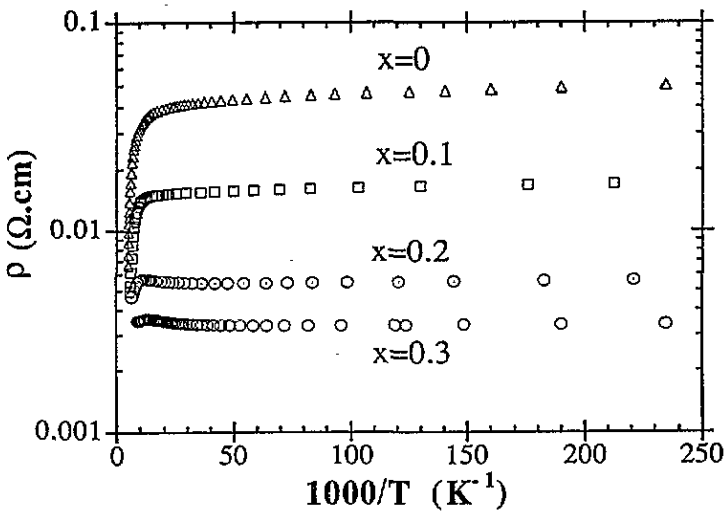

Figure 6. ρ against $1000/T$ for $Nd_{1-x}La_xNiO_{3-\delta}$ ($x \leqslant 0.3$) in the heating run.

conductivity must be related to differences in carrier mobility. Consequently, the band width must increase with the La content in the samples, in agreement with a previous band calculation [9].

3.3.2. Non-metallic phase. The resistivity of the non-metallic phase shows semiconducting behaviour at temperatures below the MI transition in samples with $x \leqslant 0.3$. The $\ln\rho$ values versus $1/T$ for $Nd_{1-x}La_xNiO_3$ samples with $x \leqslant 0.3$ between 4.2 K and the MI transition temperature, in the heating run, are plotted in figure 6. The curves are far from being straight lines, showing a continuous curvature with a striking change of slope around 50–70 K. This slope change is stronger for samples with lower La content. This result indicates the strong variation of activation energy (E_a) with the temperature. An activation energy of 990 K has been calculated for $NdNiO_3$ just below the MI transition from the curve derivative. This value can be considered an approximate estimation of the semiconducting gap for this compound. As the La content increases the semiconducting gap decreases. The values obtained are 590 K, 85 K and 15 K for samples with $x = 0.1$, $x = 0.2$ and $x = 0.3$ respectively. Furthermore, at 4.2 K all samples show small values of E_a with

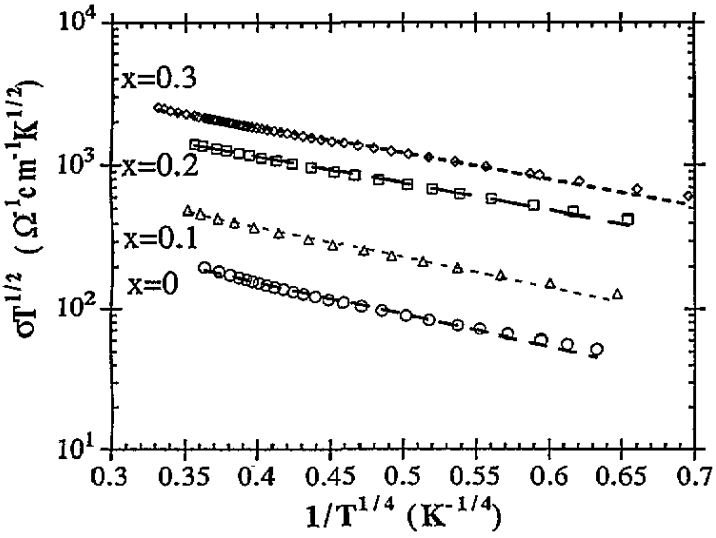

Figure 7. $\sigma T^{1/2}$ versus $1/T^{1/4}$ for $Nd_{1-x}La_xNiO_{3-\delta}$ ($x \leqslant 0.3$) and the best fit curves to equation (2) for temperatures below 70–90 K.

values close to 1 K. The drop of E_a when the temperature diminishes is characteristic of impurity conduction or polaron formation [21, 27].

Following Mott's suggestion [21], the experimental data were fitted to the expression

$$\sigma = \sigma_0 \exp[-(T_0/T)^{1/4}]. \tag{2}$$

The constants σ_0 and T_0 in (2) are expressed functionally as [28]

$$\sigma_0 = e^2 a^2 \nu_{ph} N(E_F) \tag{3}$$

and

$$T_0 = \lambda \alpha^3 / k_B N(E_F) \tag{4}$$

a being the hopping distance, given by $a = [9/(8\pi\alpha k_B N(E_F)T)]$, and e the electronic charge; ν_{ph} is a phonon frequency associated with the hop (calculated from the Debye temperature to be around 10^{13} s^{-1}) and $N(E_F)$ the density of states at the Fermi level. λ is a dimensionless constant (≈ 18.1), k_B is Boltzmann's constant and α the inverse rate of fall-off of the wavefunctions associated with the localized states. In figure 7 are plotted $\sigma T^{1/2}$ against $1/T^{1/4}$ and the best fit curves to equation (2) for temperatures below 70–90 K. The best fit parameters, summarized in table 4, show that the density of states at the Fermi level, $N(E_F)$, increases with the La content. This increase is in concordance with the decrease of the semiconducting gap, correlated with the increase of Ni–O–Ni angle to 180° due to the diminution of orthorhombic distortion. It can be noted that the estimated $N(E_F)$ for $Nd_{0.7}La_{0.3}NiO_3$ is similar to that obtained for $LaNiO_3$ following band calculations [29] and one or two orders of magnitude lower than experimental values obtained from Pauli susceptibility and calorimetric studies [16, 24, 30]. Nevertheless, the large polaron radius obtained for all samples disagrees with a small-polaron model. This could indicate that the factor responsible for the conduction properties at low temperatures is the presence of impurity levels localized in the semiconducting gap or large polarons whose mobility must be similar to small polarons, as has been suggested for spin polarons in the past [15].

Table 4. Electronic parameters for $Nd_{1-x}La_xNiO_{3-\delta}$ ($x \leqslant 0.3$) samples. $\sigma_0 T^{1/2}$ (Ω^{-1} cm^{-1} K$^{1/2}$) and T_0 (K) are obtained from the fit of figure 7. The temperature range used in the fit of ΔT (K), the density of states in the Fermi level $N(E_F)$ (eV^{-1} cm^{-3}), the inverse of wavelength rate of fall-off α (cm^{-1}), the hopping distance R (cm) and the hopping activation energy W (eV) at 40 K are also given.

	$x = 0.0$	$x = 0.1$	$x = 0.2$	$x = 0.3$
$\sigma_0 T^{1/2}$	1.55×10^3	3.1×10^3	7.2×10^3	9.8×10^3
T_0	1.1×10^3	7.7×10^2	4.3×10^2	3.1×10^2
ΔT (K)	5–67	5–80	4.2–99	4.2–85
$N(E_F)$	2.3×10^{20}	1.6×10^{21}	1.5×10^{22}	3.3×10^{22}
α	1.2×10^6	1.9×10^6	3.2×10^6	6.5×10^6
R(40 K)	7.8×10^{-7}	4.3×10^{-7}	2.2×10^{-7}	1.7×10^{-7}
W(40 K)	0.002	0.0018	0.0015	0.0014

4. Discussion and conclusions

The synthesis of $Nd_{1-x}La_xNiO_3$ samples is feasible by using sol–gel procedures. The $NdNiO_3$ shows small grain size and O deficiency [12]. The replacement of Nd by La gives samples with higher grain size and O content, resulting in stoichiometric $LaNiO_3$ at $x = 1$. A change of the unit cell symmetry is observed in the series between the samples with $x = 0.4$ and $x = 0.5$.

The magnetic properties of these samples can be explained considering two contributions: a Curie–Weiss contribution from the Nd sublattice and a temperature independent contribution assigned to the Pauli paramagnetism of itinerant electrons. The latter contribution is the only one observed in $LaNiO_3$ at temperatures above 40 K. The paramagnetic susceptibility of this oxide is around one order of magnitude higher than expected from theoretical band calculations [29] and it has been explained in the frame of spin polarons ferromagnetically correlated [15]. The similar enhancement in the Pauli paramagnetism observed in all samples indicates a similar electronic correlation in the whole system.

We have not noticed any magnetic anomaly in samples with MI transitions, and no magnetic contribution from the Ni sublattice in χ_{AC} curves is observed in these samples. Therefore, in the $Nd_{1-x}La_xNiO_3$ series electronic localization and magnetic ordering probably occur simultaneously as in $NdNiO_3$ [8, 10]. At temperatures above the MI transition, no contribution from the Ni sublattice can be justified considering a metallic band of Ni e_g^* parentage. At temperatures below the transition a new magnetic arrangement resulting in a spin density wave with antiferromagnetic and ferromagnetic interactions has been reported for the $NdNiO_3$ synthesized using high O pressures [10]. Several authors claim a coincidence of the MI transition and the Néel temperature for $NdNiO_3$ and $PrNiO_3$ [6]. This coincidence together with the strong paramagnetism of the Nd sublattice can result in the surprising absence of an anomaly in the AC susceptibility curves. Nevertheless, it is difficult to explain the lack of magnetic anomaly for the whole series on the basis of a classical spin ordering and, considering the high value of the Pauli paramagnetism contribution, it points to the existence of high magnetic correlations in the high-temperature phase.

The phase diagram of the MI transition against the average RE–O bond in the $Nd_{1-x}La_xNiO_3$ system is shown in figure 8. As the La content increases the MI transition temperature decreases. Therefore, the samples with rhombohedral unit cell are metallic in the whole temperature range. The data from previous works on samples sintered at high O

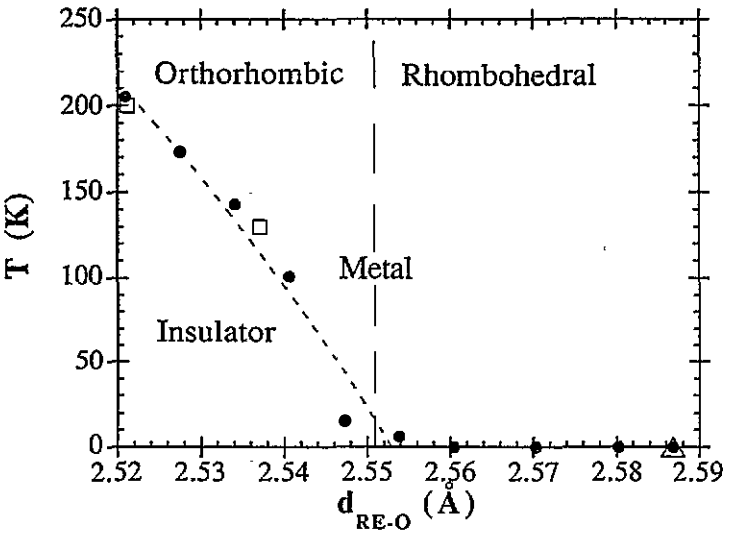

Figure 8. The phase diagram of the MI transition temperature against average RE–O distance in the $Nd_{1-x}La_xNiO_3$ system. The short-dashed line (- - - -) separates the metallic and insulator phases while the long-dashed line (– – –) separates samples with orthorhombic or rhombohedral unit cells. Experimental data, taken from experimental works [5, 6] on $NdNiO_3$ (circles), $PrNiO_3$ (squares) and $LaNiO_3$ (triangle) sintered at high O pressures, are also plotted in the figure.

pressures [5, 6] have been plotted in the same figure 8 and they are in agreement with our own results. This behaviour has been explained in terms of a correlation between the electronic properties of the samples and the Ni–O–Ni angle between adjacent octahedra. This angle determines the conduction bandwidth [9], which decreases for higher orthorhombic distortion of the unit cell, resulting in higher transition temperatures.

The linear temperature dependence of the resistivity in the metallic phase suggests a diffusive mechanism of the current carriers [21]. A dependence of resistivity following a $T^{3/2}$ power law at low temperatures is observed for samples with high La content. The $T^{3/2}$ law is characteristic of a non-degenerate gas where the resistivity is due to collisions with phonons [26], suggesting the diffusive mechanism at low temperatures. Another possibility is that electron–electron interactions become more important at low temperatures. These interactions give a T^2 power law for the resistivity, as has been reported for $LaNiO_3$ at very low temperatures [23]. We have not observed the T^2 power law in our samples but it usually appears at temperatures below 4 K [24], below our experimental range. Taking into account the electron interactions, the $T^{3/2}$ law observed for these samples could be associated with an intermediate behaviour between the linear and the T^2 law. In a recent study of $LaNiO_{3.2}$ such behaviour has been reported: the T^2 law at temperatures below a $T^{3/2}$ law in the resistivity curves [16].

Samples with low La content have a semiconducting phase at low temperatures as does $NdNiO_3$. This phase has a temperature dependent activation energy, characteristics of impurity conduction. At temperatures below 70–90 K the conduction mechanism follows a variable-range hopping mechanism. The coupling of electrons with the phonons or magnons, polarons or spin polarons would be responsible for this behaviour. The analysis of the low-temperature resistivity data leads to reasonable values for the density of states at the Fermi level $N(E_F)$. An increase of $N(E_F)$ is observed with increasing La content, which is correlated with a diminution of the charge transfer gap. On the other hand, the polaron's

radius obtained for these samples is meaningless for a small polaron. An explanation might be that the Fermi level lies in a narrow impurity band situated in the semiconducting gap for $NdNiO_3$. The impurity conduction is preponderant at low temperatures and is produced by the motion of the carriers between localized states by a variable-range hopping mechanism. When Nd is substituted by La, the diminution of semiconducting gap produces a partial overlapping of the valence and conduction bands with the impurity band increasing the density of states at the Fermi level. For higher La content, the density is so high that metallic behaviour is observed in the full temperature range. On the other hand, $LaNiO_3$ is a highly correlated metal [9] whose electron properties have been explained in the frame of spin polaron formation [15]. The spin polaron formation might also explain the linear temperature dependence of the resistivity at high temperatures and the high paramagnetic susceptibility shown by these samples. The suggestion that spin polarons with larger radii could have similar mobilities to small polarons [31] might open the question about the role, if any, of spin polaron localization in the electrical properties of $Nd_{1-x}La_xNiO_3$ at low temperatures. More experimental work, such as magnetoresistance measurements, is in progress in order to investigate this possibility.

Acknowledgments

This work was supported by CICYT projects MAT 93-0240-C04-04 and PB92-1077. The authors express their thanks to M G Proietti for a critical reading of the manuscript.

References

[1] Canfield P C, Thompson J D, Cheong S-W and Rupp L W 1993 *Phys. Rev.* B **47** 12357
[2] García-Muñoz J L, Rodríguez-Carvajal J, Lacorre P and Torrance J B 1992 *Phys. Rev.* B **46** 4414
[3] Lacorre P, Torrance J B, Pannetier J, Nazzal A I, Wang P W and Huang T C 1991 *J. Solid. State. Chem.* **91** 225
[4] Huang T C, Parrish W, Toroya H, Lacorre P and Torrance J B 1990 *Mater. Res. Bull.* **25** 1091
[5] Demazeau G, Marbeauf A, Pouchard M and Hagenmuller P 1971 *J. Solid State Chem.* **3** 582
[6] Torrance J B, Lacorre P, Nazzal A I, Ansaldo E J and Niedermayer Ch 1992 *Phys. Rev.* B **45** 8209
[7] Zaanen J, Sawatzky G A and Allen J W 1985 *Phys. Rev. Lett.* **55** 418
[8] Medarde M, Fontaine A, García-Muñoz J L, Rodríguez-Carvajal J, de Santis M, Sacchi M, Rossi G and Lacorre P 1992 *Phys. Rev.* B **46** 14975
[9] Barman S R, Chainani A and Sarma D D 1994 *Phys. Rev.* B **49** 8475
[10] García-Muñoz J L, Rodríguez-Carvajal J and Lacorre P 1992 *Europhys. Lett.* **20** 241
[11] Vassiliou J K, Hornsbostel M, Ziebarth R and Disalvo F J 1989 *J. Solid State Chem.* **81** 208
[12] Blasco J, Castro M and García J 1994 *J. Phys.: Condens. Matter* **6** 5875
[13] García J, Proietti M G, Blasco J and Benfatto M 1994 *Proc. XAFS VIII Conf. (Berlin); Physica* B at press
[14] Goodenough J B 1971 *Prog. Solid State. Chem.* **5** 276
[15] Goodenough J B, Mott N F, Pouchard M and Demazeau G 1973 *Mater. Res. Bull.* **8** 647
[16] Xu X Q, Peng J L, Li Z Y, Ju H L and Greene R L 1993 *Phys. Rev.* B **48** 1112
[17] Blasco J, García J, Proietti M G and Chaboy J 1993 *Solid State Ion.* **63–65** 585
[18] Blasco J and García J 1993 *Solid State Ion.* **63–65** 593
[19] Rillo C, Lera F, Badía A, Angurel L A, Bartolomé J, Palacio F, Navarro R and van Duynevelt A J 1991 *Magnetic Susceptibility of Superconductors and other Spin Systems* (New York: Plenum) pp 1–24
[20] Warren B F and Bodenstein P 1966 *Acta Crystallogr.* **20** 602
[21] See, for example,
Mott N F 1990 *Metal–Insulator Transitions* (London: Taylor & Francis)
Mott N F and Davis E A 1979 *Electronic Processes in Non-Crystalline Materials* (Oxford: Oxford University Press)

[22] Obradors X, Paulius L M, Maple M B, Torrance J B, Nazzal A I, Fontcuberta J and Granados Z 1993 *Phys. Rev.* B **47** 12353
[23] Sreedhar K, Honig J M, Darwin M, McElfresh M, Shand P M, Xu J, Crooker B C and Spalek J 1992 *Phys. Rev.* B **46** 6328
[24] Rajeev K P, Shivashankar G V and Raychaudhur A K 1991 *Solid State Commun.* **79** 1112
[25] Mott N F 1990 *Adv. Phys.* **39** 55
[26] Mott N F 1993 *J. Phys.: Condens. Matter* **5** 3487
[27] Springthorpe A J, Austin I G and Austin B A 1965 *Solid State Commun.* **3** 143
[28] Paul D K and Mitra S S 1973 *Phys. Rev. Lett.* **31** 1000
[29] Kemp J P and Cox P A 1990 *Solid State Commun.* **75** 731
[30] Sánchez R D, Causa M T, Sereni J, Vallet-Regí M, Sayagués M J and González Calvet J M 1993 *J. Alloys Compounds* **191** 287
[31] See for example von Malnar S and Methfessel S 1967 *J. Appl. Phys.* **38** 959
Kasuya T, Yanese A and Takeda T 1970 *Solid State Commun.* **8** 1551